

# Thermodynamic Properties and Transport Coefficients of CO<sub>2</sub>–Cu Thermal Plasmas

Aijun Yang<sup>1</sup> · Yang Liu<sup>1</sup> · Linlin Zhong<sup>1</sup> · Xiaohua Wang<sup>1</sup> ·  
Chunping Niu<sup>1</sup> · Mingzhe Rong<sup>1</sup> · Guohui Han<sup>2</sup> ·  
Youpeng Zhang<sup>2</sup> · Yanhui Lu<sup>2</sup> · Yi Wu<sup>1</sup>

Received: 31 January 2016 / Accepted: 10 April 2016 / Published online: 29 April 2016  
© Springer Science+Business Media New York 2016

**Abstract** This paper presents the calculated values of equilibrium compositions, thermodynamic properties and transport coefficients (viscosity, electrical conductivity and thermal conductivity) for CO<sub>2</sub>–Cu thermal plasmas. With several copper mass proportions, the calculation is performed at temperatures 2000–30,000 K and various pressures 0.1–16 bar. Gibbs free energy minimization is used to determine species compositions and thermodynamic properties and the well-known Chapman–Enskog method is applied to calculating transport properties. Furthermore, great attention is paid to cope with the interactions between all the particles in the determination of collision integrals. The results are illustrated indicating the effect of the copper proportions and pressure on the fundamental properties of CO<sub>2</sub>–Cu thermal plasmas. It can be found that a small quantity of copper (less than 10 %) can significantly modify the charged species densities and electrical conductivity especially at low temperature. While for other properties, the influences can be noticeable only when the copper proportion is above 10 %.

**Keywords** Thermal plasma · Thermodynamics properties · Chapman–Enskog method · CO<sub>2</sub>–Cu · Transport coefficient

---

✉ Xiaohua Wang  
xhw@mail.xjtu.edu.cn

✉ Mingzhe Rong  
mzrong@mail.xjtu.edu.cn

<sup>1</sup> State Key Laboratory of Electrical Insulation and Power Equipment, Xi'an Jiaotong University, No 28 Xianning West Road, Xi'an 710049, Shaanxi Province, People's Republic of China

<sup>2</sup> Pinggao Group Co. Ltd., Pingdingshan 467001, Henan Province, People's Republic of China

## Introduction

Thermal plasma are widely adopted by numerous industrial applications, for example, arc welding [1], arc lighting [2], circuit breakers [3, 4], plasma cutting [5] and plasma spraying [6]. In the above applications, evaporation of electrode leads to a large quantity of metal vapour in the arc. For instance, Wilhelm et al. [7] observed a metal vapour molar fraction in the center of gas metal arc welding (GMAW) above 25 % for Ar–O<sub>2</sub> mixtures and 75 % for CO<sub>2</sub> gas. Schnick et al. [8] found the molar fraction of a metal vapour above 60 % in the arc axis when studying a GMAW arc at 450 A. Liao et al. [9] simulated the electrode erosion on SF<sub>6</sub> arc. They found the Cu concentration nearby the anode upstream contact was particularly prominent for around 65 %. These metallic impurities dramatically affect characteristics of arc [10] as a result of that it modifies the thermodynamic, radiative and transport properties of the plasma. Andanson and Cheminat found the temperature near the anode decrease by up to 2000 K with the copper vapour mole fraction up to 0.4 % in 15 and 30 A argon arcs [11]. Cheminat et al. [12] discovered that when copper vapour exits with mole fraction up to 1 %, the temperature near the anode decreased by approximate 2000 K in 20–50 A argon arcs. Adachi et al. [13] discovered that adding iron with a mole fraction between 3 and 5 % lowered the arc voltage from approximate 110 to approximate 90 V for arc currents from 10 to 60 A. Rong et al. [14] concluded that, during arc motion, the voltage of arc column considering electrode erosion was smaller than that without considering electrode erosion. Lee et al. [15] discovered that, for Ag–CdO and Ag–C contacts, poor performance of gap-recovery at a current of 5 kA was mainly due to the droplets formed during arcing. Yang et al. [16] have shown that the splitting process was fundamentally changed by the existence of metal vapor. In order to investigate arc characteristics in welding and circuit breakers through magnetic hydro-dynamics, it is, therefore, imperative to calculate the thermal plasma properties considering the existence of metal vapour. This paper focuses on the transport coefficients of CO<sub>2</sub>–Cu mixtures with the motivation of the requirement of these properties for arc modelling in CO<sub>2</sub> circuit breakers and CO<sub>2</sub> welding.

A large quantity of studies can be found concerning the properties of various plasmas with metal vapour: N<sub>2</sub>–Al [17], N<sub>2</sub>–Cu [18], air–Ca/Mg/Fe [19], air–Al [20], air–Cu/Ag/Fe [21, 22], SF<sub>6</sub>–Cu [23–27], Ar–H<sub>2</sub>–Cu [28], Ar–H<sub>2</sub>–Fe [29], Ar–Cu/Fe/Al [30, 31] and He–Fe [32, 33]. Up to now, however, few papers concerning CO<sub>2</sub>–Cu mixtures can be found in spite of their importance. As for welding, CO<sub>2</sub> is widely used as a shielding gas [7, 34–36]. The metallic vapour strongly affects the weld depth in MIG welding [37] and in some cases in TIG welding [38]. As for circuit breakers, concentrated exertion has been made to seek environmental friendly media to quench arc due to the strong global warming potential of SF<sub>6</sub>. Among SF<sub>6</sub> alternatives considered, CO<sub>2</sub> has drawn particular attentions regarded as a suitable candidate [39–43]. Especially, a high-voltage circuit breaker, utilizing CO<sub>2</sub> to quench arc and insulate, has been developed by ABB company: the LTA 72D1 [44]. Using the existing data, our work focus on to attaining the consistent computed results of fundamental properties of CO<sub>2</sub>–Cu mixtures containing equilibrium compositions, thermodynamic functions and transport coefficients which are of considerable importance for the research on the CO<sub>2</sub> welding and the design optimization of CO<sub>2</sub> circuit breakers. The computation methods adopted by this work are as akin to those introduced in our earlier studies [25, 26] for SF<sub>6</sub>–Cu and thus not detailed in this paper. Special attentions are paid to the basic data required for collisions and the analysis of the main results. Here we cope with a very wide range of copper concentrations (1–100 %) (always mass proportions here)

and pressures (0.1–16 bar), meeting a majority of arc modeling requirements for welding and circuit breaker applications. Assuming only gaseous phase, the species compositions are supposed to be an equilibrium state in the temperature range 300–30,000 K. In fact, however, when the temperature is low, copper and its components exist in the mixtures primarily in the solid form since the melting temperature and the boiling temperature at atmospheric pressure of Cu is approximate 1358 and 2840 K respectively. Therefore, when the temperature is below approximately 2000 K, a mixture of CO<sub>2</sub> and copper vapour cannot be achieved as the plasma components. Therefore, our work calculated the fundamental properties of CO<sub>2</sub>–Cu mixtures in the temperature range 2000–30,000 K and all the results are presented in this temperature range which has been adopted by Cressault et al. [20, 21].

The paper is organized as follows. “[Equilibrium Compositions and Thermodynamic Properties](#)” section describes the computation of species compositions and thermodynamic properties of CO<sub>2</sub> plasma mixed with Cu vapour. “[Collision Integrals](#)” section presents an introduction of Chapman–Enskog method and potential models adopted to deal with different particle interactions to determine collision integrals which are required to compute transport coefficients. “[Transport Coefficients](#)” section presents transport coefficients under various copper concentration and pressure. Finally, conclusions are drawn in “[Conclusion](#)” section.

## Equilibrium Compositions and Thermodynamic Properties

Thermodynamic functions and transport coefficients are calculated from particle compositions of thermal plasmas. The equilibrium compositions are calculated assuming local thermodynamic equilibrium (LTE) and utilizing the Gibbs free energy minimization method. The calculation method is given in Refs. [45, 46] and has been used in our previous studies [26, 42, 43, 47]. Furthermore, Debye–Hückel correction is considered to

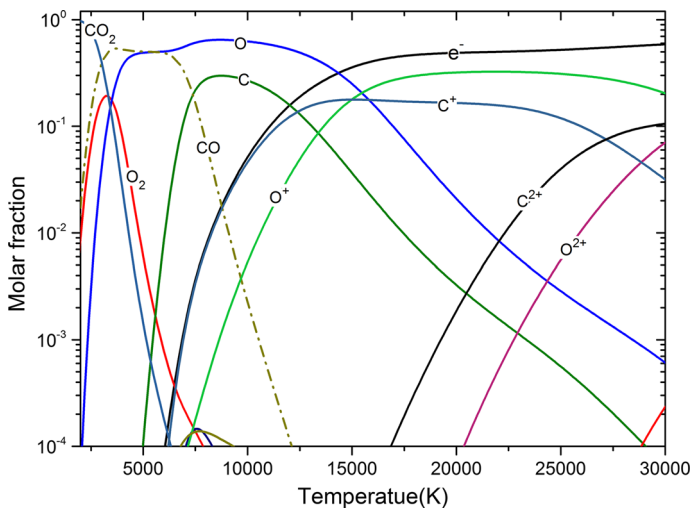


**Fig. 1** Equilibrium compositions for pure CO<sub>2</sub> gas at temperatures of 2000–30,000 K and a pressure of 1 bar

represent the extra influence of electrostatic interactions between ions. In this paper, 44 species are considered for CO<sub>2</sub>–Cu mixtures: e<sup>-</sup>, C, O, Cu, Cu<sub>2</sub>, O<sub>2</sub>, O<sub>3</sub>, C<sub>2</sub>, C<sub>3</sub>, C<sub>4</sub>, C<sub>5</sub>, CO, CO<sub>2</sub>, C<sub>2</sub>O, C<sub>3</sub>O<sub>2</sub>, CuO, C<sup>+</sup>, O<sup>+</sup>, Cu<sup>+</sup>, C<sup>2+</sup>, O<sup>2+</sup>, CO<sup>+</sup>, O<sup>3+</sup>, CO<sup>2+</sup>, C<sup>2+</sup>, O<sup>2+</sup>, Cu<sup>2+</sup>, C<sup>3+</sup>, O<sup>3+</sup>, Cu<sup>3+</sup>, C<sup>4+</sup>, O<sup>4+</sup>, Cu<sup>4+</sup>, Cu<sup>5+</sup>, Cu<sup>6+</sup>, C<sup>-</sup>, O<sup>-</sup>, Cu<sup>-</sup>, C<sub>2</sub><sup>-</sup>, O<sub>2</sub><sup>-</sup>, CO<sup>-</sup>, C<sub>3</sub><sup>-</sup>, O<sub>3</sub><sup>-</sup> and CO<sup>2-</sup>. With regard to atoms and their positive ions, the required thermodynamic data are calculated using the internal partition functions. All the basic parameters of the calculation of partition functions were compiled from NIST–JANAF tables [48]. For other species, thermodynamic data are obtained in literature [49].

Figures 1 and 2 present the equilibrium compositions for pure CO<sub>2</sub> gas and for mixtures containing 1 % of Cu, respectively. At low temperature plasma is dominated obviously by gaseous molecules. As temperature increases, gaseous molecules (such as CO<sub>2</sub>, CO and O<sub>2</sub>) dissociate into atoms (such as C and O). It is notable that the predominant positive ions are influenced remarkably by the existence of copper especially at low temperature owing to the fact that copper has relatively low ionization energy of (7.726 eV for Cu). For example, Cu<sup>+</sup> is the predominant positive ion for CO<sub>2</sub>–Cu mixtures rather than C<sup>+</sup> for pure CO<sub>2</sub> gas at around 7000 K, as is consistent with SF<sub>6</sub>–Cu [23, 26] and air–Fe [21] mixtures.

Based on equilibrium compositions, thermodynamic properties can be calculated by the standard formulas [26]. Figure 3 presents the calculated values of mass density versus temperature for CO<sub>2</sub>–Cu mixtures with several copper proportions at 1 bar. It can be observed that mass density decreases monotonically as temperature rises, which can be explained by the pressure conservation and the rarefaction effect. Mass density, at a given temperature and pressure, increases with the rising Cu proportion in CO<sub>2</sub>–Cu mixtures, which is simply due to the mass density of elementary atomic constituents (64 for Cu, 12 for C and 16 for O). The evolution of mass density for 90 %CO<sub>2</sub>–10 %Cu mixtures with different pressures is illustrated in Fig. 4. Obviously, for a given temperature, the dissociation reactions are delayed leading to the heavier molecules staying longer and the increasing pressure enhances the number density resulting in the increase of mass density.

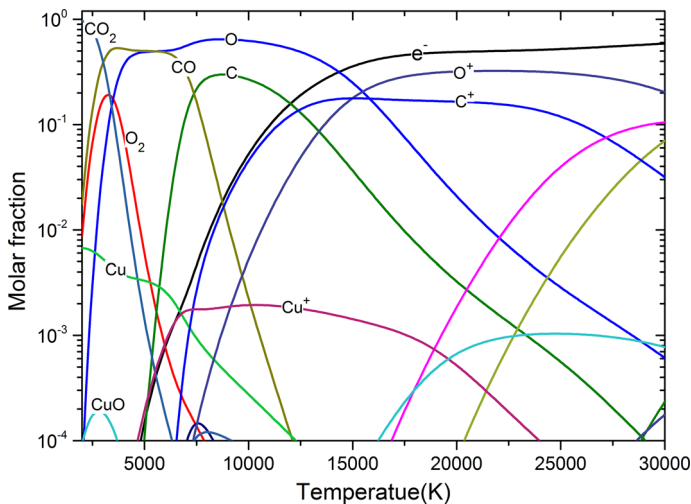


**Fig. 2** Equilibrium compositions for 90 %CO<sub>2</sub>–1 %Cu mixtures (in mass proportions) at temperatures of 2000–30,000 K and a pressure of 1 bar

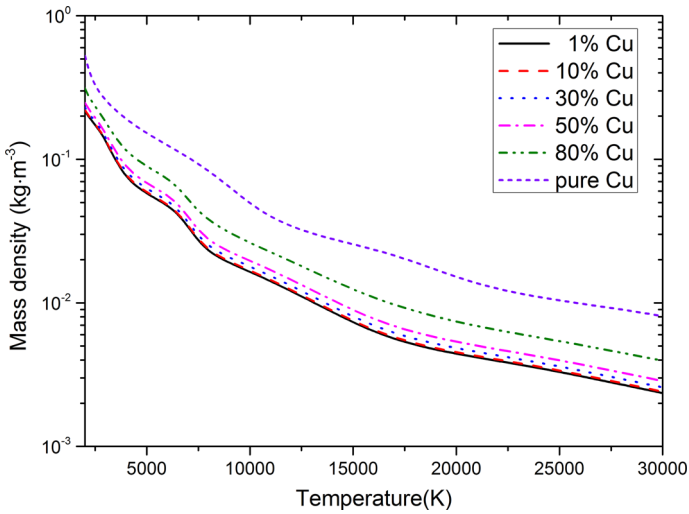


**Fig. 3** Mass density of CO<sub>2</sub>-Cu mixtures (in mass proportions) at 1 bar

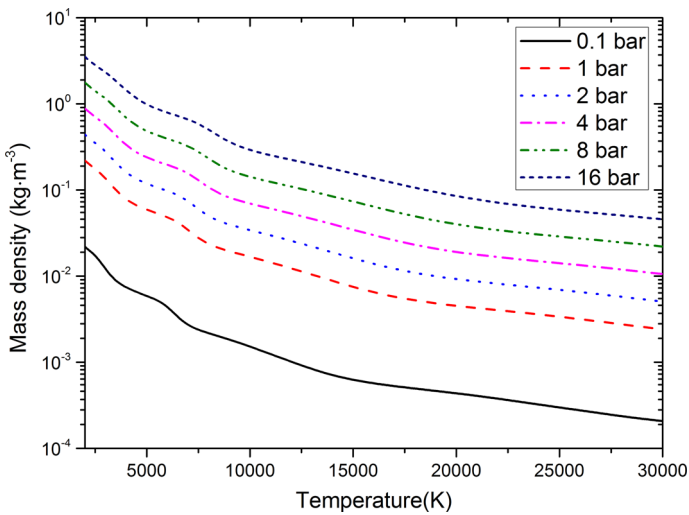


**Fig. 4** Influence of pressure on the mass density for the 90 %CO<sub>2</sub>-10 %Cu mixtures (in mass proportions)

Figure 5 presents the variation of specific heat at constant pressure for various copper proportions in CO<sub>2</sub>-Cu mixtures. It can be observed that specific heat has a significant dependence on the mix ratio and has multiple peaks. For pure CO<sub>2</sub>, the peaks at 3500 and 7300 K correspond to the dissociation of CO<sub>2</sub> and CO, respectively, while the peak at around 15,000 K is associated with the ionization of atom C and O. For pure copper, the peaks at 9800 and 19,700 K are associated with the sequential ionizations of Cu. With regard to CO<sub>2</sub> mixed with Cu vapour, the peaks are lower than those for pure CO<sub>2</sub>. 1 %Cu has little effect on the specific heat of CO<sub>2</sub> plasma. Similar to SF<sub>6</sub>-Cu mixtures [26], the

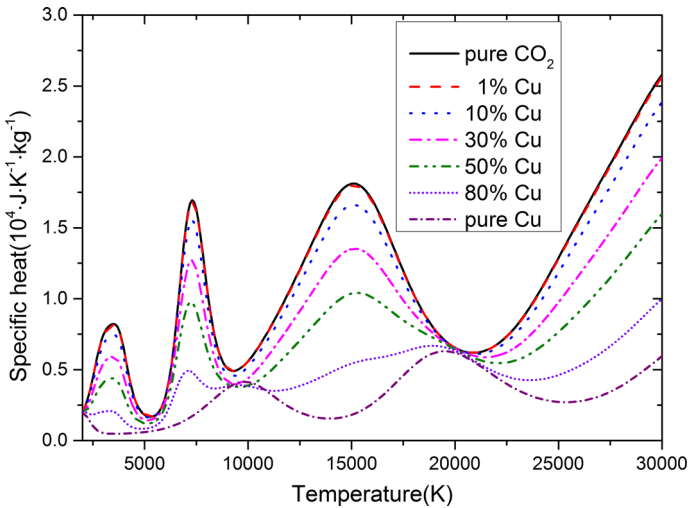


**Fig. 5** Specific heat of  $\text{CO}_2$ -Cu mixtures (in mass proportions) at 1 bar

addition of copper (above 10 %) can significantly reduce  $C_p$  especially around the peaks, due partially to the enhanced mass density.

Figure 6 illustrates the variation of  $C_p$  with various pressures for 90 % $\text{CO}_2$ -10 %Cu mixtures. When the pressure is increased, the curve peaks associated with the reactions of dissociation and ionization are removed to the higher temperature and at the same time their amplitudes are decreased. According to the Le Chatelier's principle, at a fixed temperature, rising pressure will suppress the chemical reactions such as dissociation and ionization.

## Collision Integrals

Transport coefficients are computed by the resolution of Boltzmann equation based on the classical Chapman-Enskog method, detailed in our previous studies [43]. The most difficult part in the calculation is to deal with all binary elastic collisions and compute collision integrals depending on the cross-sections. With regard to interactions in  $\text{CO}_2$  mixed with Cu, the collisions between different particles are treated as follows.

### Neutral-Neutral Interactions

There have been various potentials have been developed to describe the neutral-neutral interactions such as the exponential repulsive potential [50], the Morse potential [51], the Lennard-Jones potential [52] and the Hulburt-Hirschfelder potential [53]. Capitelli et al. [54] developed a new potential model named the Lennard-Jones like phenomenological potential, which can be used in the whole interaction range compared with these potentials. Therefore, for neutral-neutral interactions, the collision integrals are calculated with the Lennard-Jones like phenomenological potential, as has been detailed in our previous studies [25, 43]. Such potential model uses a few fundamental physical properties (polarizability  $\alpha$ , charge, number of electrons effective in polarization) to describe the

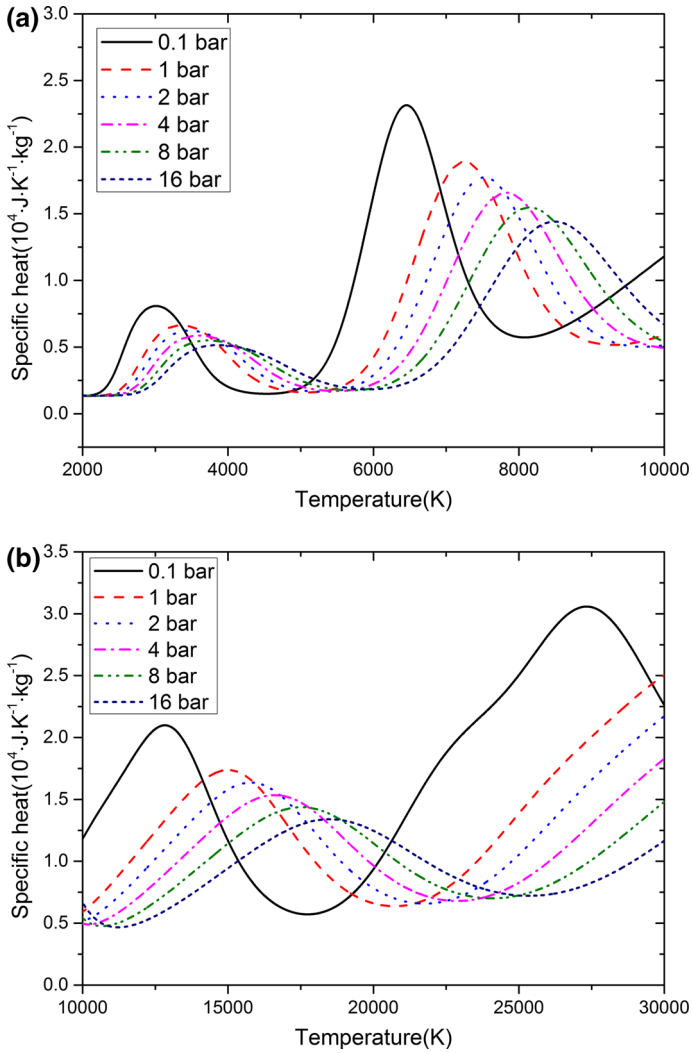


**Fig. 6** Influence of pressure on the specific heat for 90 %CO<sub>2</sub>–10 %Cu mixtures (in mass proportions)

**Table 1** Polarizability values of neutral species (Å<sup>3</sup>)

Species	Polarizability	Species	Polarizability
C	1.760	O <sub>2</sub>	1.562
O	0.802	C <sub>2</sub>	7.815
O <sub>3</sub>	2.684	C <sub>4</sub>	7.512
C <sub>3</sub>	5.179	CO	1.953
C <sub>5</sub>	11.164	C <sub>2</sub> O	4.087
CO <sub>2</sub>	2.507	C <sub>3</sub> O <sub>2</sub>	6.873
Cu	6.2	Cu <sub>2</sub>	11.554
CuO	4.658		

interaction energy. Table 1 presents the polarizability data used in this paper obtained from the NIST Computational Chemistry Comparison and Benchmark Database [55].

### Neutral–Ion Interactions

Both the elastic collision and the charge-exchange inelastic collision should be both taken into account when dealing with neutral–ion interactions, which was detailed in our previous work [43].

For elastic collision, the polarization potential model has been widely used for calculating elastic collision integrals [56]. The phenomenological potential model is preferred in this paper with the fact that it has been developed to elastic interactions between the neutral and ion [25, 43, 54]. Table 2 tabulates the polarizability of several ions which were compiled from the Computational Chemistry Comparison and Benchmark Database [55]. For the charged particles whose polarizability data are unavailable in literature, the polarization potential is adopted to compute the collision integrals for elastic interactions.

The charge-exchange inelastic collision plays a vital role in the determination of collision integrals for  $X-X^+$  interactions. Transport cross section  $Q_{ij}^{(l)}(\varepsilon)$  can be estimated through the charge transfer cross-section  $Q_{ex}$  [23, 57, 58]:

$$Q_{ij}^{(l)}(\varepsilon) = 2Q_{ex} \quad (1)$$

where  $Q_{ex}$  can be evaluated by

$$Q_{ex} = \frac{1}{2}[A - B \ln(g)]^2 \quad (2)$$

with the parameters  $A$  and  $B$ , obtained through experimental or theoretical approaches, and independent of impact velocity  $g$ . In this work, the charge-exchange inelastic collisions are considered for  $C-C^+$ ,  $O-O^+$ ,  $Cu-Cu^+$ ,  $CO-CO^+$  and  $O_2-O_2^+$  interactions. For  $C-C^+$  and  $O-O^+$  interactions, the parameters  $A$  and  $B$  can be obtained from the theoretical data  $Q_{ex}$  given by Copeland et al. [59]. For  $CO-CO^+$  and  $O_2-O_2^+$  interactions, the parameters  $A$  and  $B$  can be got from the theoretical data  $Q_{ex}$  given by Yevseyev et al. [60]. For  $Cu-Cu^+$  interaction, Mosthaghani proposed  $A = 4.74 \times 10^{-9}$  and  $B = 4.67 \times 10^{-10}$  [61], which has been adopted by some workers [21, 23, 25, 30]. However, Aubreton pointed out that the values proposed by Mosthaghani were absolutely incorrect (maybe misprint)

**Table 2** Polarizability values of ion species ( $\text{\AA}^3$ )

Species	Polarizability	Species	Polarizability
$C^+$	0.829	$C^-$	7.280
$C^{2+}$	0.578	$C^{3+}$	0.289
$C^{4+}$	0.003	$C_2^+$	3.200
$C_2^-$	3.660	$O^+$	0.376
$O^-$	3.200	$O^{2+}$	0.228
$O^{3+}$	0.182	$O^{4+}$	0.164
$O_2^+$	0.958	$O_2^-$	1.581
$O_3^-$	6.42	$CO^+$	1.341
$CO^-$	14.153	$CO_2^+$	2.212
$CO_2^-$	7.765	$Cu^+$	0.204
$Cu^-$	0.252		



because when the collision energy is around 1 eV, their work gave negative values of  $A - B \ln(g)$  [62]. Based on the collision integrals for Cu–Cu<sup>+</sup> interaction at 1000 and 5000 K, given by Bouillon [63] and Abdelhakim et al. [61], Aubreton established a non-linear system and obtained  $A = 2.454 \times 10^{-9}$  and  $B = 1.091 \times 10^{-10}$ . In this paper, the parameters  $A$  and  $B$  for Cu–Cu<sup>+</sup> interaction are obtained based on Rapp and Francis’ recommendation [64]. They developed an approximate calculation and obtained the charge transfer cross-section  $Q_{ex}$  from Eq. (3) and (4) for different atoms.

$$Q_{ex}^{\frac{1}{2}} = \left(\frac{1}{2}\pi\right)^{\frac{1}{2}} \left(\frac{a_0}{2\gamma}\right) \ln \left[ \frac{72\bar{b}_1^3}{\pi\gamma a_0} \left(\frac{I^2}{\hbar^2}\right) \left(1 + \frac{a_0}{\gamma\bar{b}_1}\right)^2 \right] - \left(\frac{1}{2}\pi\right)^{\frac{1}{2}} \left(\frac{a_0}{\gamma}\right) \ln(g) \tag{3}$$

$$\left(\frac{2\pi}{\gamma a_0}\right)^{\frac{1}{2}} \left(\frac{I}{\hbar g}\right) \bar{b}_1^{\frac{3}{2}} \left(1 + \frac{a_0}{\gamma\bar{b}_1}\right)^2 \exp\left(-\frac{\gamma\bar{b}_1}{a_0}\right) = \frac{\pi}{6} \tag{4}$$

where  $\gamma = I/13.6$ ,  $a_0$  is Bohr radius,  $I$  is the ionization potential in electron volt,  $\hbar$  is reduced Planck constant,  $\bar{b}_1$  is the average  $b_1$  obtained from Eq. (4) for a limited range of  $g$ . Based on (3) and (4), we can get  $A = 2.278 \times 10^{-9}$  and  $B = 8.797 \times 10^{-11}$ . Table 3 gives the constants  $A$  and  $B$  considered in this paper to characterize the charge exchange cross sections.

### Electron–Neutral Interactions

As for interactions between the electron and neutral, the collision integrals are obtained by straightforward integration of  $Q_{ij}^{(0)}(\varepsilon)$ . The treatment of electron–neutral interactions involving CO<sub>2</sub> species (C, O, C<sub>2</sub>, O<sub>2</sub>, CO and CO<sub>2</sub>) is detailed in our previous study [43]. As for e–Cu interaction, the collision integrals are obtained from Ref. [66]. According to Cressault’s recommendation [21], the potential of polarizability is adopted to deal with the e–Cu<sub>2</sub> and e–CuO interactions.

### Charged–Charged Interactions

A screened Coulomb potential is often used to describe the charged–charged interactions. However, when dealing with the Debye shielding effect, there are some debates about whether both the heavy particles and electrons or only electrons should be considered. Recently, Ghorui et al. [67] proposed a revised definition of the shielding Debye length for charged–charged interactions in two-temperature non-equilibrium plasma, which considers both ions and electrons but assumes they have the same temperature which means they are under the local thermal equilibrium (LTE). It should be stressed that when thermal plasma is assumed to be LTE (adopted by this work), the revised shielding length proposed by

**Table 3** The constants  $A$  and  $B$  for the approximation of charge-exchange cross sections (Å)

Interaction	A	B	Data source
C–C <sup>+</sup>	22.7338	1.2837	[59]
Cu–Cu <sup>+</sup>	22.78	0.8797	[64]
O–O <sup>+</sup>	20.1794	1.1383	[65]
O <sub>2</sub> –O <sub>2</sub> <sup>+</sup>	17.1453	0.9233	[60]
CO–CO <sup>+</sup>	20.4702	1.0629	[47]

Ghorui et al. is same to the previous shielding length considering both ions and electrons. Here, we mention that this study follows the recommendation of Murphy [68] and does not consider ions when calculating the Debye length.

## Transport Coefficients

### Electrical Conductivity

The electrical conductivity  $\sigma$  is computed based on Deveto's study [69] to the third approximation of the Chapman–Enskog method. It should be mentioned that only the electrons' contribution is taken into account when calculating  $\sigma$  because electrons' mobility is higher than charged species.

Since some literatures have investigated the fundamental properties for pure  $\text{CO}_2$  and pure Cu plasmas, some comparisons are made to validate our calculations. For pure  $\text{CO}_2$ , our results, compared with different authors' theoretical results, shows a good agreement, and have been discussed in our previous study [43]. For pure Cu plasma, we validate our results of electrical conductivity through compared with those of Cressault et al. [21] at 1 bar, as plotted in Fig. 7. It is apparent that, in the whole temperature range considered, our results agree well with those of Cressault et al. [21].

The evolution of electrical conductivity for  $\text{CO}_2$ –Cu mixtures with various Cu concentrations is illustrated in Fig. 8. For temperature below 7500 K, it can be observed that minimal Cu in  $\text{CO}_2$ –Cu mixtures powerfully increases the electrical conductivity due to a lower ionization energy of Cu atom (7.726 eV for Cu) compared with those of carbon and oxygen neutral species (11.2603 eV for C, 13.6181 eV for O). The behavior can be also seen in air–metal (Cu, Ag, Fe, and Al) [20, 21] and Ar–metal (Cu, Fe and Al) [30] mixtures. It should be mentioned that the electrical conductivity of  $\text{CO}_2$ –Cu mixtures shows an opposite variation when the rising Cu concentration at high temperature (above

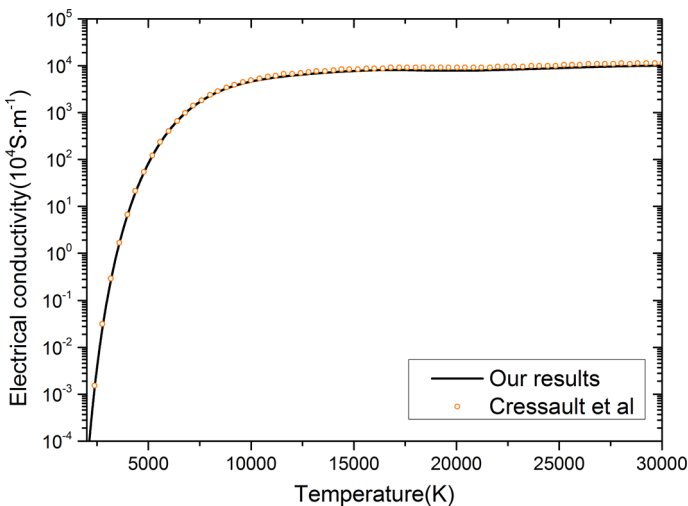


**Fig. 7** Electrical conductivity of pure Cu at 1 bar. The calculated results of Cressault et al. [21] are shown for comparison

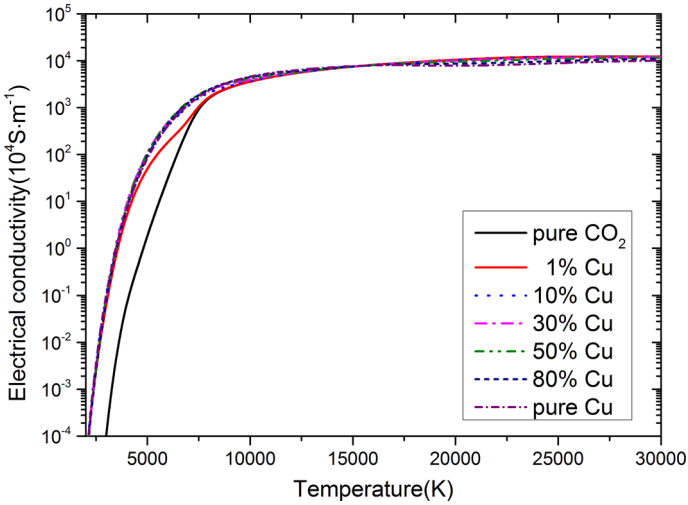


**Fig. 8** Electrical conductivity in CO<sub>2</sub>-Cu mixtures with different Cu proportions (in mass proportions) at temperatures up to 30,000 K and a pressure of 1 bar

15,000 K), despite the electron number density (not shown in this paper) increasing with the copper proportion. This behavior can be explained by the reason that, in this temperature range, increasing the Cu concentration results in more multiple-charged particles formed due to a low ionization energy of Cu atom. As we know, the electrical conductivity is proportional to electron mobility and electron density. For charged–charged interactions, the fact that collision integrals of multiple-charged ions are higher, leads to a lower electron mobility and thus a lower electrical conductivity.

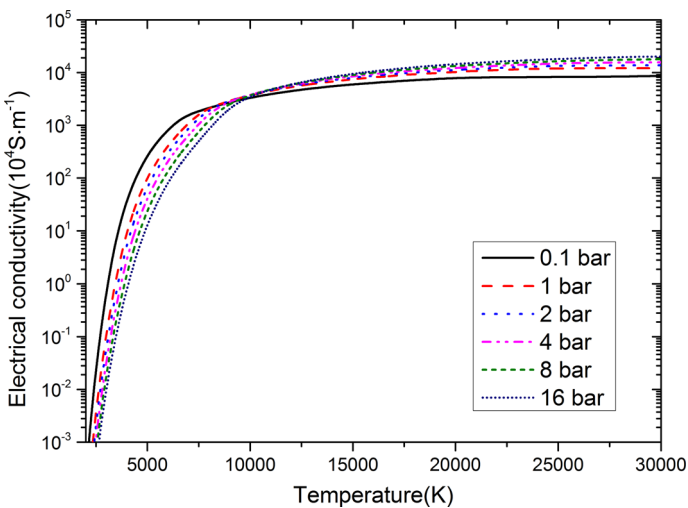
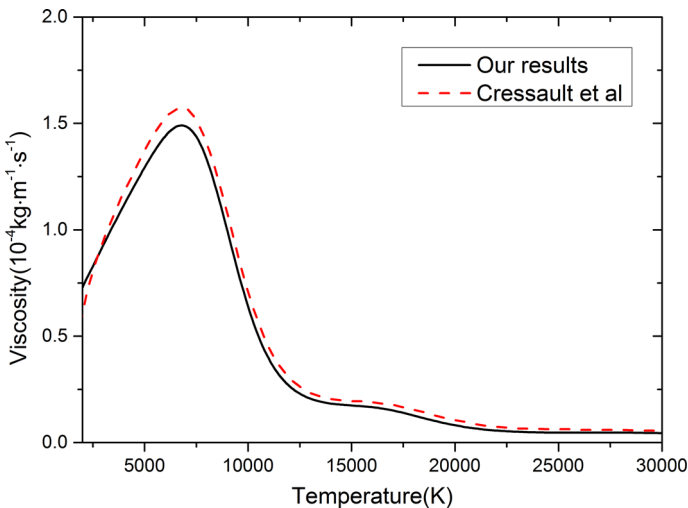


**Fig. 9** Electrical conductivity in 90 %CO<sub>2</sub>-10 %Cu mixtures (in mass proportions) at various pressures

The evolution of electrical conductivity for CO<sub>2</sub>–Cu mixtures under various gas pressures is illustrated in Fig. 9. At low temperature (below 10,000 K), increasing pressure causes a decrease in electrical conductivity. However, at high temperature, the opposite effect is noted. It should be noted that, at a fixed temperature, increasing gas pressure will enhance the electron number density continuously (not presented in this paper). A similar performance has been reported for SF<sub>6</sub>–Cu [25], air–metal [20] and CO<sub>2</sub>–C<sub>2</sub>F<sub>4</sub> [43] mixtures. This performance is mainly due to the evolution of main elastic collisions involving electrons. At low temperature, electron–neutral interactions are mainly responsible for the collision integrals. The electrical conductivity can be written as a first approximation:  $\sigma \propto n_e / \left( \sum_{i \neq e} n_i \bar{\Omega}_{ei} \right)$ , based on the formula given by Devoto [69]. When increasing of the gas pressure, the ionization is suppressed and the electron density does not increase rapidly as other neutral species, leading to the decrease of electrical conductivity. At high temperature (above 10,000 K), electron–ion interactions become predominant. The ionization is delayed by the increasing pressure and hence lowers the density of high valence ions, leading to a rise of electrical conductivity.

## Viscosity

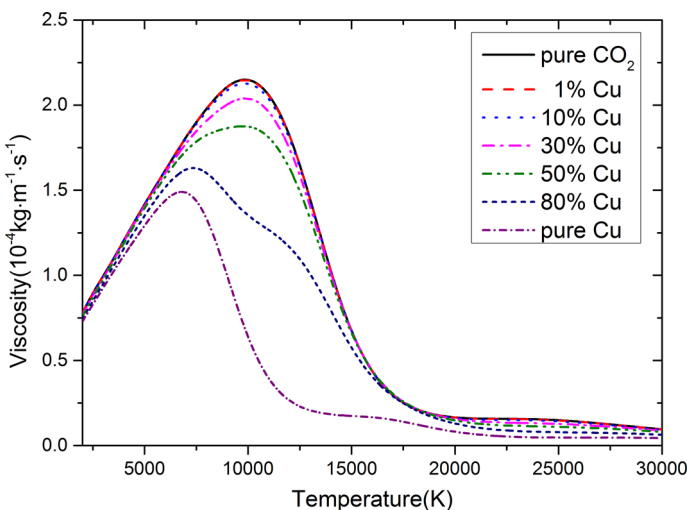
The viscosity  $\eta$ , as usual, is assumed to be independent of electron properties, which on physical grounds is acceptable for that a particle's viscosity is proportional to the mass [70]. It is calculated with a first approximation of the method of Chapman–Enskog. The evolution of viscosity for pure Cu at 1 bar is presented in Fig. 10, compared with those of Cressault et al. [21]. A good agreement, except a little higher peak around 6000 K, can be observed. The small discrepancies are mainly due to the collision integrals obtained from diverse methods. For instance, The Lennard-Jones potential was adopted by Cressault et al. to describe neutral species interactions while Lennard-Jones like phenomenological potential by us.



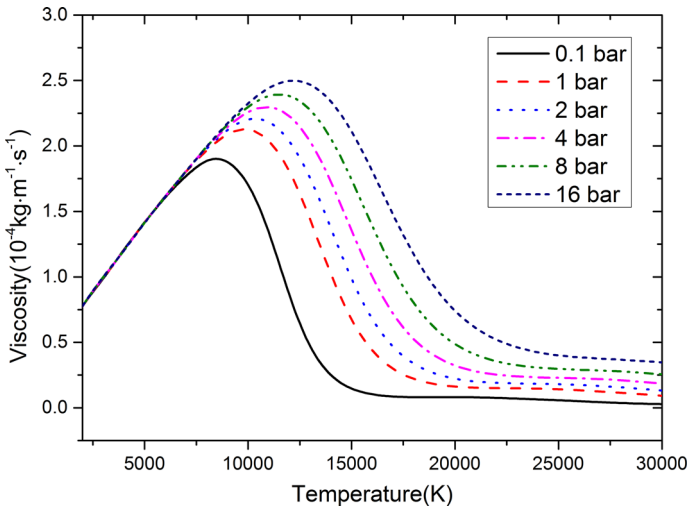
**Fig. 10** Viscosity of pure Cu at 1 bar. The calculated results of Cressault et al. [21] are shown for comparison

Figure 11 presents the influence of Cu proportions on the viscosity. Besides being directly proportional to  $\sqrt{M_i M_j T / (M_i + M_j)}$  ( $M$  is molar weight), the viscosity of the thermal plasma is inversely proportional to the collision integrals  $\bar{\Omega}_{ij}^{(2,2)}$ . It is noted that the predominant collision integrals  $\bar{\Omega}_{xx}^{(2,2)}$  increase with temperature when neutral–neutral collisions control, but decrease when ion–ion collisions dominate resulted from the large collision integrals. Thus, the curve peak of viscosity represents a change in the elastic collisions from neutral–neutral collisions dominating to ion–ion collisions dominating between heavy particles in CO<sub>2</sub>–Cu mixtures. Besides, the presence of Cu vapour for mass proportions below 10 % shows little impact on the viscosity. Therefore, the viscosity of pure CO<sub>2</sub> can be applied to approximate the viscosities of CO<sub>2</sub>–Cu mixtures with small proportions of Cu vapour. This behaviour is rather distinct from that of the electrical conductivity. It can be also observed that the viscosity decreases with copper proportion (above 10 %) especially at temperatures of 5000–15,000 K. This is attributed to the increase of neutral–neutral collision integrals  $\Omega_{ij}^{(2,2)}$  with an addition of Cu.

The variation of viscosity for CO<sub>2</sub>–Cu mixtures under different gas pressure is highlighted in Fig. 12. First, it can be seen that the viscosity is almost independent on the pressure when temperature is below 7000 K, since the viscosity, compared with other parameters, is more sensitive to temperature at temperature below 7000 K. Besides, as can be also observed that the viscosity increases with pressure when the temperature is above 7000 K. This is attributed to the suppression of ionization caused by increasing pressure which leads to a declined collision integrals by Coulomb potentials. Finally, there is a phenomenon that, for a larger pressure, the viscosity peaks are shifted to a higher temperature. This behavior can be illustrated by the reason that increasing pressure suppresses the ionization and the powerful Coulomb interactions will dominate at higher temperature.



**Fig. 11** Viscosity in CO<sub>2</sub>–Cu mixtures with various Cu proportions (in mass proportions) 1 bar



**Fig. 12** Viscosity in 90 %CO<sub>2</sub>–10 %Cu mixtures (in mass proportions) with various pressures

### Thermal Conductivity

Thermal conductivity  $\kappa$  is consisted of three components: internal thermal conductivity  $\kappa_{int}$  the translational thermal conductivity  $\kappa_{tr}$  (containing  $\kappa_{tr}^h$  from heavy particles and  $\kappa_{tr}^e$  from electrons), and reaction thermal conductivity  $\kappa_{react}$  [23]. A second-order approximation of Chapman–Enskog method is adopted to compute internal thermal conductivity  $\kappa_{int}$  which describes transport of internal energy.  $\kappa_{tr}^e$  and  $\kappa_{tr}^h$  can be calculated according to third-order and second-order approximations of Chapman–Enskog method, respectively. The reaction

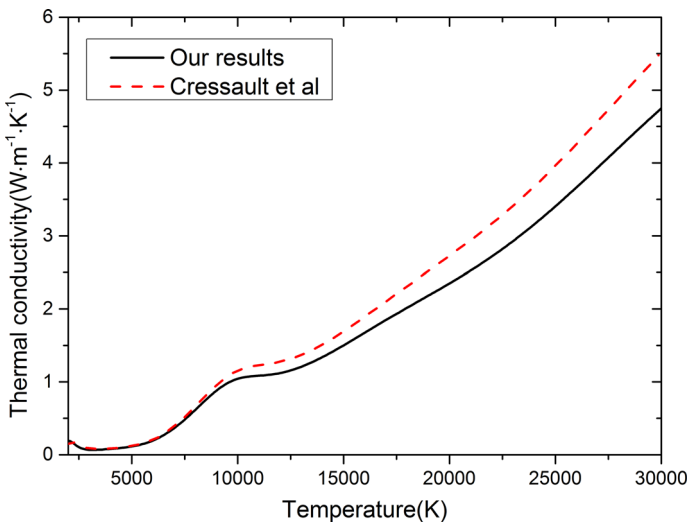
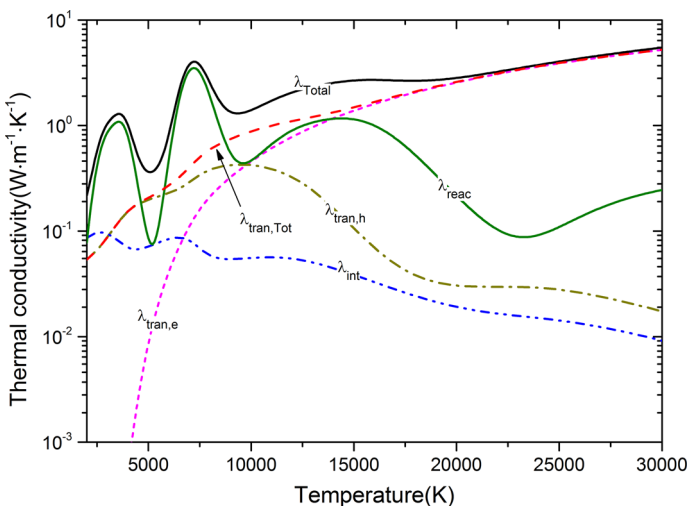


**Fig. 13** Thermal conductivity of pure Cu at 1 bar. The calculated results of Cressault et al. [21] are shown for comparison

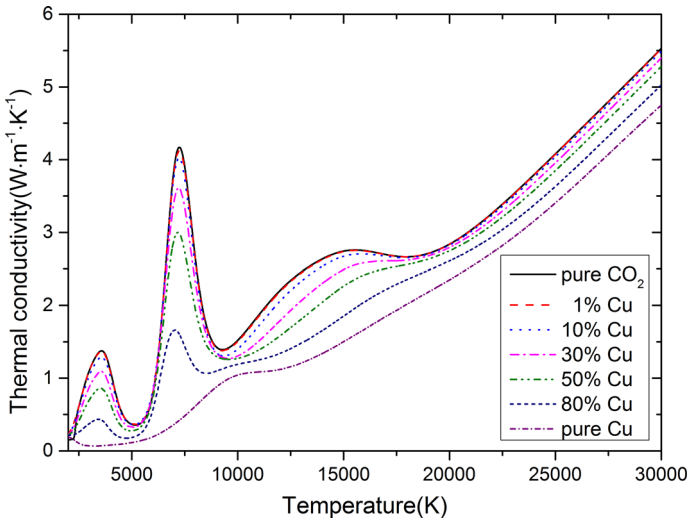
thermal conductivity  $\kappa_{\text{reac}}$  represents the transport of energy by dissociation and recombination of molecules and ionization of species. It is computed by the expressions derived firstly by Butler and Brokaw [71] for neutral gas mixtures and then developed to ionized mixtures by Meador and Stanton [72]. The calculation of thermal conductivity is validated by comparing with those obtained by Cressault et al. [21] for pure Cu, shown in Fig. 13. The discrepancies mainly occur above 8000 K. At around 10,000 K, this difference is caused by different charge exchange cross sections of Cu–Cu + interaction. Above 15,000 K, the discrepancies can be attributed to the different definitions of the Debye length. Heavy particles were taken into account by Cressault et al. in the Debye shielding effect, whereas ions are not considered in this study following the recommendation of Murphy and Arundell [58].

Figure 14 shows the components of thermal conductivity of 90 %CO<sub>2</sub>–10 %Cu mixtures (mass proportions) at 1 bar. It can be observed that the internal thermal conductivity  $\kappa_{\text{int}}$  can be neglected during the temperatures range considered in this work. The reaction thermal conductivity  $\kappa_{\text{reac}}$  is rather essential as a result of incessant dissociation and ionization reactions, particularly below 15,000 K. The reactions of CO<sub>2</sub> and its resultants considered to calculate the reaction thermal conductivity can be found in our previous work [43], while for Cu and its resultants, the successive ionization of Cu and the dissociation of Cu<sub>2</sub> are taken into consideration. Below 10,000 K, translational contribution of heavy particles is rather significant with an upward trend but, above 10,000 K, decreases with temperature since ionization occurs. The translational contribution of electrons rising monotonically with temperature exceeds that of heavy species and reaction thermal conductivity at temperature above 10,000 and 14,500 K, respectively. Above 20,000 K, as the gas is mightily ionized, the thermal conductivity is dominated by the elastic collisions between ions and electrons. Therefore,  $\kappa_{\text{tr}}^e$  is predominant and other components can be neglected.

The impact of Cu proportions on the thermal conductivity of CO<sub>2</sub>–Cu mixtures is illustrated in Fig. 15. The several peaks which are akin to those of specific heat (presented in Fig. 5) correspond to the reactions of dissociation and ionization. The peaks' positions



**Fig. 14** Components of thermal conductivity of 90 %CO<sub>2</sub>–10 %Cu mixtures (in mass proportions) at 1 bar



**Fig. 15** Thermal conductivity in  $\text{CO}_2$ -Cu mixtures with different Cu proportions (in mass proportions) with temperatures up to 30,000 K and a pressure of 1 bar

and amplitudes are mighty dependent on the Cu proportions due to the complicated reactions in the mixtures. Indeed, the peaks' amplitude is attenuated when increasing the Cu concentration, since the ionization of Cu need less energy and easier than the dissociation of  $\text{CO}_2$  species and ionization of atomic carbon and oxygen. It is also can be observed that minimal concentration of Cu vapour (below 10 %) weakly change the thermal conductivity of  $\text{CO}_2$ -Cu mixtures, as is akin to that observed of viscosity. The

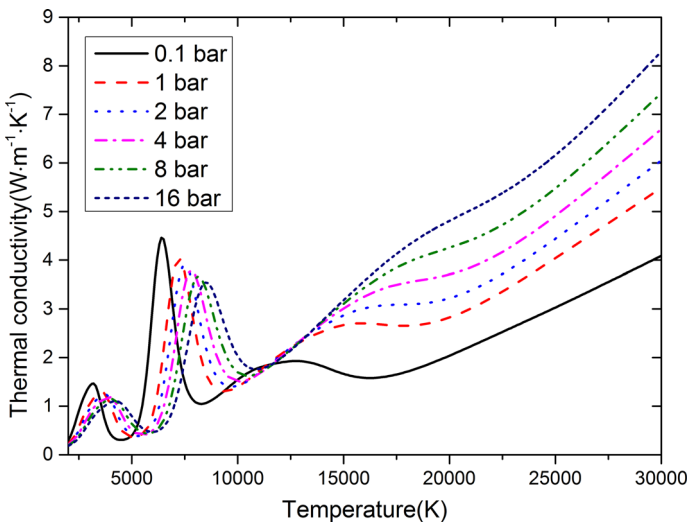


**Fig. 16** Thermal conductivity in 90 % $\text{CO}_2$ -10 % Cu mixtures (in mass proportions) at temperatures up to 30,000 K and various pressures



evolution of thermal conductivity for CO<sub>2</sub>–Cu mixtures with different gas pressures is presented in Fig. 16. Increasing pressure will remove the peaks of the thermal conductivity to a higher temperature with decreased amplitudes. Similar to the specific heat, this behavior can be explained by the suppressed chemical reactions and variation of species compositions.

## Conclusion

In this paper, the fundamental properties, containing the equilibrium compositions, thermodynamic properties and transport coefficients (viscosity, electrical conductivity and thermal conductivity) of high-temperature CO<sub>2</sub>–Cu mixtures for several copper concentrations are computed at pressures of 0.1–16 bar and temperatures of 2000–30,000 K. The Lennard-Jones like phenomenological potential is utilized to compute collision integrals of all neutral–neutral interactions and partial neutral–ion interactions for ions with available polarizability data in literature and the polarization potential is adopted for the remaining ion–neutral interactions. Some updated transport cross sections are used to compute electron–neutral collision integrals.

The calculation of transport coefficients is confirmed through compared with the finite results available of other authors. Special attentions are paid on investigating the evolution of fundamental properties of CO<sub>2</sub>–Cu mixtures with different copper proportions. A small quantity of copper can significantly modify the charged species densities resulting from the low ionization energy of Cu. Electrical conductivity is therefore enhanced due to the existence of Cu, especially at low temperature. It should be noted that the addition of copper has an opposite effect on the electrical conductivity of CO<sub>2</sub>–Cu mixtures when temperature is high (above 15,000 K) due to the higher densities of multi-charge ions. The other properties, however, is not sensitive to the presence of a small percentage of Cu copper. All the thermal plasma properties can be significantly changed when the copper proportion is elevated (above 10 %). The impact of pressure on various properties is also discussed and classical results are obtained.

To our knowledge, our calculation fills the lack of the data related to the thermodynamic properties and transport coefficients of high-temperature CO<sub>2</sub>–Cu mixtures which are not available in the literature before. These calculated results is vital for the arc modelling in CO<sub>2</sub> welding and CO<sub>2</sub> circuit breakers. In the arc welding, the metal vapour has a significant influence on the depth of the weld the transport of energy to the work piece and. For a circuit breaker, when there is a decaying arc, the high electrical conductivity at low temperatures may enhance the restrike and therefore decrease the interruption capability.

**Acknowledgments** This work was supported by National Key Basic Research Program of China (973 Program) (2015CB251002), National Natural Science Foundation of China (No. 51521065 and 51221005), China Postdoctoral Science Foundation (2015M572558) and the State Key Laboratory of Electrical Insulation and Power Equipment (No. EIPE16307).

## References

1. Tanaka M, Lowke JJ (2007) Predictions of weld pool profiles using plasma physics. *J Phys D Appl Phys* 40:R1–R23
2. Franck CM, Seeger M (2006) Application of high current and current zero simulations of high-voltage circuit breakers. *Contrib Plasma Phys* 46(10):787–797

3. Swierczynski B, Gonzalez JJ, Teulet P, Freton P, Gleizes A (2004) Advances in low-voltage circuit breaker modelling. *J Phys D Appl Phys* 37:595–609
4. Nemchinsky VA, Severance R (2006) What we know and what we do not know about plasma arc cutting. *J Phys D Appl Phys* 39:R423–R438
5. Fauchais P (2004) Understanding plasma spraying. *J Phys D Appl Phys* 37:R86–R108
6. Lister GG, Lawler JE, Lapatovich WP, Godyak VA (2004) The physics of discharge lamps. *Rev Mod Phys* 76:541–598
7. Wilhelm G, Gött G, Schöpp H, Uhrlandt D (2010) Study of the welding gas influence on a controlled short-arc GMAW process by optical emission spectroscopy. *J Phys D Appl Phys* 43(43):434004
8. Schnick M, Füssel U, Hertel M, Spille-Kohoff A, Murphy AB (2010) Metal vapour causes a central minimum in arc temperature in gas–metal arc welding through increased radiative emission. *J Phys D Appl Phys* 43(2):022001
9. Liao VK, Lee BY, Song KD, Park KY (2006) The influence of contacts erosion on the SF<sub>6</sub> arc. *J Phys D Appl Phys* 39(10):2114
10. Murphy AB (2010) The effects of metal vapour in arc welding. *J Phys D Appl Phys* 43(43):434001
11. Andanson P, Cheminat B (1979) Contamination d'un plasma d'argon par des vapeurs anodiques de cuivre. *Rev Phys Appl* 14(8):775–782
12. Cheminat B, Gadaud R, Andanson P (1987) Vaporisation d'une anode en argent dans la plasma d'un arc électrique. *J Phys D Appl Phys* 20(4):444–452
13. Adachi K, Inaba T, Amakawa T (1991) Voltage of wall-stabilized argon arc injected with iron powder. In: *Proceeding 10th international symposium plasma chemistry*, Bochum, Germany, 4–9 Aug 1991, 1, pp 3–10
14. Rong M, Ma Q, Wu Y, Xu T, Murphy AB (2009) The influence of electrode erosion on the air arc in a low-voltage circuit breaker. *J Appl Phys* 106(2):023308
15. Lee A, Herberlein JVR, Meyer TN (1985) High-current arc gap with ablative wall: dielectric recovery and wall-contact interaction. *IEEE Trans Compon Hybrids Manuf Technol* 8(1):129–134
16. Yang F, Rong M, Wu Y, Murphy AB, Pei J, Wang L, Liu Z, Liu Y (2010) Numerical analysis of the influence of splitter-plate erosion on an air arc in the quenching chamber of a low-voltage circuit breaker. *J Phys D Appl Phys* 43(43):434011
17. Abdelhakim H, Dinguirard JP, Vacquie S (1980) The influence of copper vapour on the transport coefficients in a nitrogen arc plasma. *J Phys D Appl Phys* 13(8):1427
18. Dassanayake MS, Etemadi K (1989) Thermodynamic and transport properties of an aluminum–nitrogen plasma mixture. *J Appl Phys* 66(11):5240–5244
19. Tanaka Y, Yokomizu Y, Kato M, Matsumura T, Shimizu K, Takayama S, Okada T (1997) Electrical and thermal conductivities and enthalpy of air plasma contaminated with Fe, Ca, Mg or H<sub>2</sub>O vapour. In: P Fauchais (ed) *The 4th international thermal plasma processes conference*, Athens, Greece, 15–18 July 1996, Begell House, New York, 1997, pp 587–594
20. Cressault Y, Gleizes A, Riquel G (2012) Properties of air–aluminum thermal plasmas. *J Phys D Appl Phys* 45:265202
21. Cressault Y, Hannachi R, Teulet Ph, Gleizes A, Gonnet J-P, Battandier J-Y (2008) Influence of metallic vapours on the properties of air thermal plasmas. *Plasma Sources Sci Technol* 17:035016
22. Cressault Y, Gleizes A (2010) Calculation of diffusion coefficients in air–metal thermal plasmas. *J Phys D Appl Phys* 43:434006
23. Chervy B, Gleizes A, Razafinimanana M (1994) Thermodynamic properties and transport coefficients in SF<sub>6</sub>–Cu mixtures at temperatures of 300–30 000 K and pressures of 0.1–1 MPa. *J Phys D Appl Phys* 27:1193
24. Krenek P (1992) Thermophysical properties of the reacting mixture SF<sub>6</sub> and Cu in the range 3000 to 50 000 K and 0.1 to 2 MPa. *Acta Technol CSAV* 37:399–410
25. Wang XH, Zhong LL, Cressault Y, Gleizes A, Rong MZ (2014) Thermophysical properties of SF<sub>6</sub>–Cu mixtures at temperatures of 300–30,000 K and pressures of 0.01–1.0 MPa: part 2. Collision integrals and transport coefficients. *J Phys D Appl Phys* 47:495201
26. Rong MZ, Zhong LL, Cressault Y, Wang XH, Chen F, Zheng H (2014) Thermophysical properties of SF<sub>6</sub>–Cu mixtures at temperatures of 300–30 000 K and pressures of 0.01–1.0 MPa: part 1. Equilibrium compositions and thermodynamic properties considering condensed phases. *J Phys D Appl Phys* 47:495202
27. Zhong L, Wang X, Rong M, Wu Y, Murphy AB (2014) Calculation of combined diffusion coefficients in SF<sub>6</sub>–Cu mixtures. *Phys Plasmas* 21:103506
28. Cressault Y, Gleizes A (2004) Thermodynamic properties and transport coefficients in Ar–H<sub>2</sub>–Cu plasmas. *J Phys D Appl Phys* 37:560–572

29. Essoltani A, Proulx P, Boulos MI, Gleizes A (1994) Effect of the presence of iron vapors on the volumetric emission of Ar/Fe and Ar/Fe/H<sub>2</sub> plasmas. *Plasma Chem Plasma Process* 14:301–315
30. Cressault Y, Murphy AB, Teulet Ph, Gleizes A, Schnick M (2013) Thermal plasma properties for Ar–Cu, Ar–Fe and Ar–Al mixtures used in welding plasmas processes: II. Transport coefficients at atmospheric pressure. *J Phys D Appl Phys* 46:415207
31. Cressault Y, Gleizes A (2013) Thermal plasma properties for Ar–Al, Ar–Fe and Ar–Cu mixtures used in welding plasmas processes: I. Net emission coefficients at atmospheric pressure. *J Phys D Appl Phys* 46:415206
32. Murphy AB, Tanaka M, Yamamoto K, Tashiro S, Sato T, Lowke JJ (2009) Modelling of thermal plasmas for arc welding: the role of the shielding gas properties and of metal vapour. *J Phys D Appl Phys* 42:194006
33. Tashiro S, Tanaka M, Nakata K, Iwao T, Koshiishi F, Suzuki K, Yamazaki K (2007) Plasma properties of helium gas tungsten arc with metal vapour. *Sci Technol Weld Join* 12:202–207
34. Lu S, Fujii H, Nogi K (2008) Marangoni convection and weld shape variations in He–CO<sub>2</sub> shielded gas tungsten arc welding on SUS304 stainless steel. *J Mater Sci* 43:4583–4591
35. Tanaka M, Tashiro S, Ushio M, Mita T, Murphy AB, Lowke JJ (2006) CO<sub>2</sub>-shielded arc as a high-intensity heat source. *Vacuum* 80:1195–1198
36. Hoffmann T, Baldea G, Riedel U (2009) Thermodynamics and transport properties of metal/inert-gas mixtures used for arc welding. *Proc Combust Inst* 32:3207–3214
37. Murphy AB (2013) Influence of metal vapour on arc temperatures in gas–metal arc welding: convection versus radiation. *J Phys D Appl Phys* 46:224004
38. Tanaka M, Yamamoto Y, Tashiro S, Nakata K, Yamamoto E, Yamazaki K, Suzuki K, Murphy AB, Lowke JJ (2010) Time-dependent calculations of molten pool formation and thermal plasma with metal vapour in gas tungsten arc welding. *J Phys D Appl Phys* 43:434009
39. Stoller PC, Seeger M, Iordanidis AA, Naidis GV (2013) CO<sub>2</sub> as an Arc Interruption Medium in Gas Circuit Breakers. *IEEE Trans Plasma Sci* 41:2359–2369
40. Uchii T, Shinkai T, Suzuki K (2002) Thermal interruption capability of carbon dioxide in a puffer-type circuit breaker utilizing polymer ablation. *Proc IEEE/PES Trans Distrib Conf Exhib Asia Pacific* 3:1750–1754
41. Wada J, Ueta G, Okabe S (2013) Evaluation of breakdown characteristics of CO<sub>2</sub> gas for non-standard lightning impulse waveforms-breakdown characteristics in the presence of bias voltages under non-uniform electric field. *IEEE Trans Dielectr Electr Insul* 20:112–121
42. Zhong LL, Yang AJ, Wang XH, Liu DX, Wu Y, Rong MZ (2014) Dielectric breakdown properties of hot SF<sub>6</sub>-CO<sub>2</sub> mixtures at temperatures of 300–3500 K and pressures of 0.01–1.0MPa. *Phys Plasmas* 21:053506
43. Yang A, Liu Y, Sun B, Wang X, Cressault Y, Zhong L, Rong M, Wu Y, Niu C (2015) Thermodynamic properties and transport coefficients of high-temperature CO<sub>2</sub> thermal plasmas mixed with C<sub>2</sub>F<sub>4</sub>. *J Phys D Appl Phys* 48:495202
44. LTA 72D1 CO<sub>2</sub> high voltage circuit breaker. <http://www.ABB.com/highvoltage>
45. Murphy AB (2001) Thermal plasmas in gas mixtures. *J Phys D Appl Phys* 34:R151
46. Gleizes A, Gonzalez JJ, Freton P (2005) Thermal plasma modelling. *J Phys D Appl Phys* 38:R153
47. Wang X, Zhong L, Yan J, Yang A, Han G, Han G, Wu Y, Rong M (2015) Investigation of dielectric properties of cold C<sub>3</sub>F<sub>8</sub> mixtures and hot C<sub>3</sub>F<sub>8</sub> gas as Substitutes for SF<sub>6</sub>. *Eur Phys J D* 69(10):1–7
48. Chase MW, Davies CA Jr (1998) NIST–JANAF thermochemical tables, 4th edn. American Institute of Physics for the National Institute of Standards and Technology, New York
49. Burcat A, Ruscic B (2005) Third millennium ideal gas and condensed phase thermochemical database for combustion with updates from active thermochemical tables (Argonne National Laboratory), Report number ANL-05/20. <http://www.chem.leeds.ac.uk/combustion/combustion.html>
50. Monchick L (1959) Collision integrals for the exponential repulsive potential. *Phys Fluids* 2:695–700
51. Smith FJ, Munn RJ (1964) Automatic calculation of the transport collision integrals with tables for the morse potential. *J Chem Phys* 41:3560–3568
52. Neufeld PD, Janzen AR, Aziz RA (1972) Empirical equations to calculate 16 of the transport collision integrals (l, s)\* for the Lennard Jones (12–6) potential. *J Chem Phys* 57:1100–1102
53. Rainwater JC, Holland PM, Biolsi L (1982) Binary collision dynamics and numerical evaluation of dilute gas transport properties for potentials with multiple extrema. *J Chem Phys* 77:434–437
54. Laricchiuta A, Colonna G, Bruno D, Celiberto R, Gorse C, Pirani F, Capitelli M (2007) Classical transport collision integrals for a Lennard-Jones like phenomenological model potential. *Chem Phys Lett* 445:133–139
55. NIST Computational Chemistry Comparison and Benchmark Database, NIST Standard Reference Database Number 101 Release 16a, June 2015, Editor: Russell D. Johnson III. <http://cccbdb.nist.gov/>

56. André P, Bussiere W, Rochette D (2007) Transport coefficients of Ag–SiO<sub>2</sub> plasmas. *Plasma Chem Plasma Process* 27:381–403
57. Wang WZ, Murphy AB, Yan JD, Rong AZ, Spencer JW, Fang MTC (2012) Thermophysical properties of high-temperature reacting mixtures of carbon and water in the range 400–30,000 K and 0.1–10 atm. Part 1: equilibrium composition and thermodynamic properties. *Plasma Chem Plasma Process* 32:75–96
58. Murphy AB, Arundell CJ (1994) Transport coefficients of argon, nitrogen, oxygen, argon–nitrogen, and argon–oxygen plasmas. *Plasma Chem Plasma Process* 14:451–490
59. Copeland FBM, Crothers DSF (1997) Cross sections for resonant charge transfer between atoms and their positive ions. *At Data Nucl Data Tables* 65:273–288
60. Yevseyev AV, Radtsig AA, Smirnov BM (1982) The asymptotic theory of resonance charge exchange between diatomics. *J Phys B At Mol Phys* 15:4437–4452
61. Abdelhakim H, Dinguirard JP, Vacquie S (1980) The influence of copper vapour on the transport coefficients in a nitrogen arc plasma. *J Phys D Appl Phys* 13:1427
62. Aubreton A, Elchinger MF (2003) Transport properties in non-equilibrium argon, copper and argon–copper thermal plasmas. *J Phys D Appl Phys* 36:1798
63. Bouillon Combadiere S (1995) Etude d'un plasma d'air ensemencé de vapeurs de cuivre: propriétés de transport, diagnostiques et interaction avec des matériaux. Doctoral dissertation
64. Rapp D, Francis WE (1962) Charge exchange between gaseous ions and atoms. *J Chem Phys* 37:2631–2645
65. Rutherford JA, Vroom DA (1974) The reaction of atomic oxygen with several atmospheric ions. *J Chem Phys* 61:2514–2519
66. Zatsarinny O, Bartschat K (2010) Electron collisions with copper atoms: elastic scattering and electron-impact excitation of the  $(3\ d\ 10\ 4\ s)\ 2\ S \rightarrow (3\ d\ 10\ 4\ p)\ 2\ P$  resonance transition. *Phys Rev A* 82:062703
67. Ghorui S, Das AK (2013) Collision integrals for charged–charged interaction in two-temperature non-equilibrium plasma. *Phys Plasmas* 20:093504
68. Murphy AB (2000) Transport coefficients of hydrogen and argon–hydrogen plasmas. *Plasma Chem Plasma Process* 20:279–297
69. Devoto RS (1967) Simplified expressions for the transport properties of ionized monatomic gases. *Phys Fluids* 10:2105–2112
70. Devoto RS (1967) Third approximation to the viscosity of multicomponent mixtures. *Phys Fluids* 10:2704–2706
71. Butler JN, Brokaw RS (1957) Thermal conductivity of gas mixtures in chemical equilibrium. *J Chem Phys* 26:1636–1643
72. Meador WE, Stanton LD (1965) Electrical and thermal properties of plasmas. *Phys Fluids* 8:1694–1703